IEEE Access
Multidisciplinary | Rapid Review | Open Access Journal

Received December 27, 2017, accepted January 3, 2018, date of publication January 11, 2018, date of current version February 28, 2018.

Digital Object Identifier 10.1109/ACCESS.2018.2791962

Risk Management of Heatstroke Based on Fast Computation of Temperature and Water Loss Using Weather Data for Exposure to Ambient Heat and Solar Radiation

KAZUYA KOJIMA[1], AKIMASA HIRATA[1], (Fellow, IEEE), KAZUMA HASEGAWA[1], SACHIKO KODERA[1], ILKKA LAAKSO[2], (Member, IEEE), DAISUKE SASAKI[3], TAKESHI YAMASHITA[3], RYUSUKE EGAWA[4], YUKA HORIE[5], NANAKO YAZAKI[5], SAERI KOWATA[5], KENJI TAGUCHI[6], AND TATSUYA KASHIWA[6], (Member, IEEE)

[1]Department of Electrical and Mechanical Engineering, Nagoya Institute of Technology, Nagoya 466-8555, Japan
[2]Department of Electrical Engineering and Automation, Aalto University, 02150 Espoo, Finland
[3]Information Technology Division, Information Department, Tohoku University, Sendai 980-8578, Japan
[4]Cyberscience Center, Tohoku University, Sendai 980-8578, Japan
[5]Japan Weather Association, Tokyo 170–6055, Japan
[6]Department of Electrical and Electronic Engineering, Kitami Institute of Technology, Kitami 090-8507, Japan

Corresponding author: Akimasa Hirata (ahirata@nitech.ac.jp)

This work was supported by the Joint Usage/Research Center for Interdisciplinary Large-scale Information Infrastructures and High Performance Computing Infrastructure in Japan under Project jh170010-NAH.

ABSTRACT Several indexes, such as the heat index, wet-bulb globe temperature, and the universal thermal climate index, are used to estimate the risk of seasonal heat illness. These indexes correspond to the heat load of an individual in identical environmental conditions for a prolonged period of time. In daily life, the environment changes with time, and different individuals are vulnerable to heat-related illness to different degrees. An appropriate health risk assessment covering 90% of the population would facilitate an effective response to increased rates of heat illness for major summer sport events and the elderly in daily life. In this paper, a fast computation for simulating temperature elevation and sweating is implemented using weather forecast data. In particular, a bioheat equation considering thermoregulatory responses is solved in the time domain using anatomical human body models including young adults, the elderly, and children. To accelerate simulation, the computational code is vectorized and parallelized, and subsequently implemented on an SX-ACE supercomputer. The computational results are validated in typical cases of young adults, children, and the elderly. The computational time for estimating the body temperature elevation and water loss for 3 h based on the forecasted temperature, humidity, and solar radiation was 8 min for a total of nine human models that cover an estimated 90% of the population. This demonstrates the effectiveness of the proposed system for pre-emptive health risk management. To improve public awareness, a web-based risk management application has been developed and used, since 2017 in Japan.

INDEX TERMS Bioheat equation, thermoregulatory response, heat stroke, decline in sweating rate.

I. INTRODUCTION

Recently, the number of fatal heat waves has been increasing in Europe, North America, and Asia. Heat waves in these areas are expected to be more intense and frequent in the second half of the 21st century [1]. In Japan, there were 6,770 fatalities due to heat stroke between 1968 and 2007 [2]. In addition, the yearly number of patients requiring emergency treatment has reached 40,000−60,000 [3].

Heat stroke cases depend on age and environment. 50% of the patients are over 65 years old, and they get illness mostly in home. In most cases, they are unaware of the risk, owing to the decline in their thermal sensitivity [4]. Other typical cases are athletes and workers [5].

As far as workers are concerned, it is quite difficult to shut-down industrial plants even when environmental temperature reaches critical levels. Moreover, it is virtually impossible

to change the schedule of major sport events (e.g., Summer Olympic Games). Thus, it is essential to effectively manage the heat-related risk of workers as well as athletes and spectators.

Several indexes, such as the heat index, wet-bulb globe temperature (WBGT) [6], and the universal thermal climate index [7], can be used to estimate heat-related risk. These indexes may be metrics of heat-related risk when an individual remains in the same environmental condition. In daily life, the environment changes with time, and the duration of heat exposure is case-specific.

For occupational scenarios, the American Conference of Government Industrial Hygienists (ACGIH) [8] has published and maintained standards for managing work duration using an empirical equation in terms of WBGT, whereby workers are assumed to wear long sleeve shirts and pants (work clothes). Thus, this may not be applied to daily life activities, such as those involving athletes and spectators. In particular, spectators are more heat sensitive because most of them are not as acclimatized as athletes. In the Summer Olympic Games, spectators account for more than 70% of the cases of heat-related illness [5].

It would be useful if highly-reliable risk assessment was possible for different and time-dependent cases and human models (age, gender, morphology, and thermoregulation capacity). A solution is to conduct simulations for specific cases covering most of the population. Then, if the analysis could be conducted in a timely manner, it could be applied to risk management.

To estimate temperature elevation, several computational models have been proposed by combining thermodynamics and thermoregulation, in addition to electromagnetics (solar radiation). Compartment-based [9], [10] or realistic anatomical models [11] are used as human body models. In this study, the latter are used owing to their flexibility in considering the body surface area-to-mass ratio, which is a dominant factor in temperature elevation by ambient temperature [12]. In addition, the thermoregulatory response is expressed in terms of core and average skin temperature elevations [9], [13]. The change (particularly for "elevation") of basal metabolic rate in exercise is mainly in muscles and is position-dependent. Thus, the use of anatomical human models is more suitable for risk evaluation. The drawback is that the computational cost for handling such models is substantial, namely, 16 h on a workstation (CPU: Intel®Xeon®W5590 @3.33GHz, 4×2 cores).

In this study, the code is vectorized and parallelized to realize fast evaluation of core temperature elevation and sweating, and is subsequently implemented on an SX-ACE supercomputer [14]. A risk assessment system for heat illness is then developed by simulating body temperature elevation and sweating combined with weather forecast data. The system can be used for public awareness, particularly for the aged and parents of small children, and for managing the risk of workers as well as athletes and spectators.

II. MODEL AND METHODS

A. HUMAN BODY MODELS

In this study, Japanese adult male and female body models and a three-year-old child model were used [15]. The adult models were divided into 51 anatomic regions (e.g., skin, muscle, bone, brain, and heart) with a resolution of 0.5 mm for electromagnetic computation, and 2 mm for temperature computation. The height, weight, and surface area of the models are summarized in Table 1. The adult male body model was used in computations for younger adults (20–30 years old), the elderly (65 years old), and the aged (75 years old), because no clear difference in body shape is observed between healthy younger and older adults. Moreover, no anatomical model for the elderly has been developed.

TABLE 1. Parameters of Anatomical Adult and Child Models

	3-year Child	Adults (Elderly)
Height [cm]	88.2	173.2
Weight [kg]	14.4	65.0
Surface area [m^2]	0.57	1.86

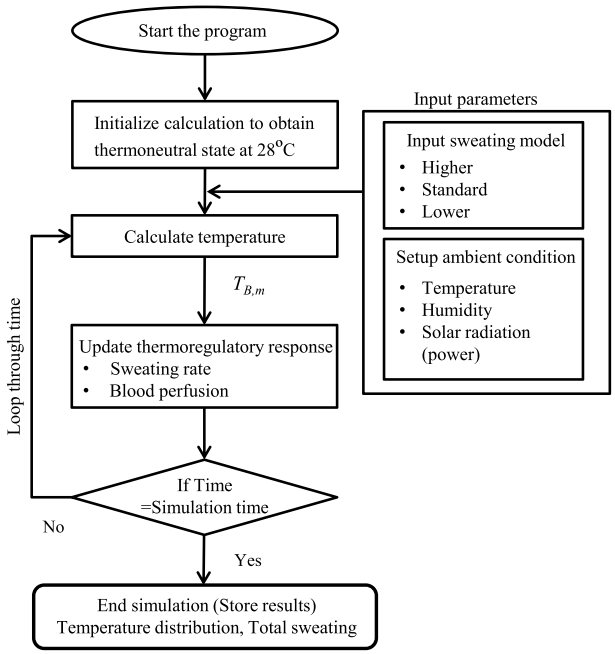

FIGURE 1. Flowchart of bioheat modeling using thermoregulatory response in computational domain.

B. THERMAL ANALYSIS

The algorithm for computing temperature variation considering thermoregulatory responses is summarized in Figure 1. The detailed formulation is presented in the following sections.

1) BIOHEAT EQUATION

The temperature elevation in the numerical human models was calculated by solving the bioheat equation [16], which models the thermodynamics of the body. A generalized bioheat equation considering thermoregulation and core temperature change [11] is

$$\begin{aligned} C(\boldsymbol{r})\,\rho(\boldsymbol{r})\,\frac{\partial T(\boldsymbol{r},t)}{\partial t} &= \nabla\cdot\left(K(\boldsymbol{r})\,\nabla T(\boldsymbol{r},t)\right)+\rho(\boldsymbol{r})\,E^2(r) \\ &\quad + M(\boldsymbol{r},t)-B(\boldsymbol{r},t)\left(T(\boldsymbol{r},t)-T_B(m,t)\right) \end{aligned} \tag{1}$$

where $T(\mathbf{r}, t)$ and $T_B(m, t)$ denote the tissue temperature and blood temperature, respectively, of different body parts (m = 1, . . . , 5, where m = 1, 2, 3, 4, and 5 represent the head and trunk, right hand, left hand, right leg, and left leg, respectively); C [J/kg/°C] is the specific heat of the tissue; σ [S/m] is the electrical conductivity of the tissue; E [V/m] is the internal electric field caused by solar radiation; K [W/m/°C] is the thermal conductivity of the tissue; M [W/m^3] is the basal metabolic rate per unit volume; and B [W/m^3/°C] is a term associated with blood perfusion.

The boundary condition between air and tissue for (1) is expressed by

$$-K(\boldsymbol{r})\,\frac{\partial T(\boldsymbol{r},t)}{\partial n}=H(\boldsymbol{r},t)\cdot\left(T(\boldsymbol{r},t)-T_e(t)\right)+EV(r)\,, \tag{2}$$

where H [W/m^2/°C], T [°C], and T_e [°C] denote the heat transfer coefficient, body surface temperature, and air temperature, respectively. H includes the convective and radiative heat loss, and EV [W/m^2] is the evaporative heat loss.

2) BLOOD (CORE) TEMPERATURE COMPUTATION

The key feature of the proposed computational modeling is that, in contrast to conventional bioheat modeling, both the body core temperature variation and the temperature in shallow regions can be tracked. To satisfy the first law of thermodynamics [17], [18], blood temperature varies according to the following equation:

$$T_B(m,t)=T_B(m,0)+\int_t\frac{Q_{B_{tot}}(m,t)\pm Q_B(m,t)}{C_B\rho_B V_B(m)}, \tag{3}$$

where Q_{Btot} is the net rate of heat acquisition of blood from the tissues in body part m, Q_B is the heat exchange between the head and trunk and one of the limbs (m = 2, 3, 4, 5), C_B (=4,000 J/kg·°C) is the specific heat of blood, ρ_B(=1, 050 kg/m^3) is the mass density, and V_B is the total blood volume in body part m. V_B [m^3] over the body is set to 7% of the weight of the corresponding body parts [17], [18]. The heat exchange between the head and trunk and one of the limbs is given in [9].

3) BIOHEAT EQUATION THERMAL PARAMETERS

The thermal constants of human tissues and the heat transfer coefficients used in this study are identical to those in [19]. The effect of these parameters on the temperature of the elderly for a compartment human body model is discussed in [20]. The heat transfer coefficient from the skin to the air, including the insensible heat loss, varies according to the following equation [21]:

$$\begin{aligned} H(\boldsymbol{r},t) &= \left(H_C(\boldsymbol{r},t)+H_R(\boldsymbol{r},t)\right)/R_{sf} \\ H_C(\boldsymbol{r},t) &= \left[a_{nat}\cdot\left(T_{sf}(t)-T_e(t)\right)^{1/2}+a_{frc}\cdot v+a_{mix}\right]^{1/2} \\ H_R(\boldsymbol{r},t) &= \sigma\cdot\psi\cdot\varepsilon_{sf}\cdot\varepsilon_{sr} \\ &\quad\times\left[\left(T_{sf}(t)+273\right)^2+\left(T_e(t)+273\right)^2\right] \\ &\quad\times\left[\left(T_{sf}(t)+273\right)+\left(T_e(t)+273\right)\right] \end{aligned} \tag{4}$$

where H_C [W/m^2/°C] is the convective heat transfer coefficient, H_R [W/m^2/°C] is the radiative heat transfer coefficient, v [m/s] is the speed of air movement, and T_{sf} [°C] is the average body surface temperature. a_{nat} (=4.63), a_{frc} (=199.74), and a_{mix} (=−9.8) are the corresponding regression coefficients. σ (=5.67 × 10^{-8} W/m^2/K^4) is the Stefan-Boltzmann constant, ψ(= 0.794) is the corresponding view factor, and ε_{sf} (=0.99) and ε_{sr} (=0.93) are the emissivity of the body surface and surrounding indoor space, respectively. The numeric phantom used is discretized by voxels; thus, its surface is approximately 1.4 times as large as that of an actual human [22]. The heat transfer coefficient is adjusted by the ratio between the actual and voxelized body surface area.

It should be noted that the blood perfusion rate in the elderly is known to be smaller than that in younger adults (e.g., 30% smaller in thermally steady state in [23]); in addition, the core temperature in thermoneutral condition is lower. Even though the core temperature in thermoneutral condition was set to 36.5 °C for the elderly with a 30% smaller blood flow, the resultant temperature elevation was almost identical. Thus, the blood flow in thermally steady state for the elderly was assumed to be identical to that for younger adults in this study.

C. THERMOREGULATORY RESPONSE IN YOUNGER AND OLDER ADULTS

1) MODELING EVAPORATIVE HEAT LOSS

The evaporative heat loss EV on the skin is

$$EV=\min\left\{SW\times 40.6/S, EV_{\max}\right\}, \tag{5}$$

where SW is the sweating rate [g/min] (see below), S [m^2] is the surface area of the human body, and the numerical factor 40.6 W·min/g is a conversion coefficient. The maximum evaporative heat loss EV_{max} on the skin depends on the ambient conditions according to the following formula [13]:

$$EV_{\max}=2.2h_c f_{pcl}(P_S-\varphi_e P_A) \tag{6}$$

where h_c is the convective heat transfer coefficient; P_S and P_A are the saturated water vapor pressure at skin temperature and at the ambient air temperature, respectively; φ_e is the relative humidity of the ambient air; and f_{pcl} is the permeation

efficiency factor of clothing, which is affected by the speed of air movement [24]. For simplicity, f_{pcl} is assumed to be 1, corresponding to a naked body.

Sweating in younger adults is modeled using the formulas in [9] and extended for the elderly. The sweating rate SW is assumed to depend on the temperature elevation on the skin and in the hypothalamus as follows:

$$SW(\boldsymbol{r}, t) = \gamma(\boldsymbol{r})\chi(\boldsymbol{r})\{W_S(\boldsymbol{r}, t)\Delta T_S(t) + W_H(\boldsymbol{r}, t)\Delta T_H(t)\} + PI \quad (7)$$

$$W_S(\boldsymbol{r}, t) = \alpha_{11}\tanh(\beta_{11}\Delta T_S(t) - \beta_{10}) + \alpha_{10}, \quad (8)$$

$$W_H(\boldsymbol{r}, t) = \alpha_{21}\tanh(\beta_{21}\Delta T_H(t) - \beta_{20}) + \alpha_{20}, \quad (9)$$

where ΔT_S and ΔT_H are the average temperature elevation of the skin and the hypothalamus, respectively, and PI (insensible water loss) is 0.63 g/min and 0.25 g/min for adults and children, respectively. The multiplier $\gamma(\boldsymbol{r})$ denotes the dependence of the sweating rate on the body parts (Table 2 in [9]). In each body part, the sweating rate is assumed to be constant. Three types of sweating intensity were considered: lower, standard, and higher, listed in Table 3. The coefficients α and β are empirically estimated for the average sweating rate [13].

TABLE 2. Dependence of Sweating Rate on Body Parts in (7).

Body part	
Head, Face	0.149
Neck	0.042
Shoulders and Thorax	0.138
Abdominal	0.181
Arms	0.133
Hands	0.049
Legs	0.261
Feet	0.047

TABLE 3. Coefficient of Sweating Rate in (8) and (9).

	Sweating Intensity		
	Lower	Standard	Higher
α_{10} [g/(min·°C)]	0.95	1.20	1.35
α_{11} [g/(min·°C)]	0.55	0.80	0.95
α_{20} [g/(min·°C)]	3.80	6.30	7.30
α_{21} [g/(min·°C)]	3.20	5.70	6.70
β_{10}	0.09	0.19	0.15
β_{11} [°C^{-1}]	0.59	0.59	0.59
β_{20}	1.80	1.03	0.47
β_{21} [°C^{-1}]	2.70	1.98	2.30

2) MODELING SWEATING IN THE ELDERLY

The maximum sweating rate in most body parts except for the limbs was shown to be almost identical in younger adults and the elderly [25]–[28]. In [29], the original formula (7) was modified as follows: i) the decline in sweating in the limbs was considered by adding a multiplier $\chi(\boldsymbol{r}) = 0.6$ in the legs, and ii) the threshold for inducing a sweating response in the elderly, which represents the decline in the thermal sensitivity of the skin owing to aging, was increased by introducing $\Delta T_{S,dec}$ and $\Delta T_{H,dec}$ (see (10)). This value was estimated to be 1.5 °C in [29].

Thus, in the model for the aged, ΔT_S and ΔT_H in (7) are given by

$$\Delta T_S = \begin{cases} 0 & T_S < T_{S,0} + \Delta T_{S,dec} \\ T_S - (T_{S,0} + \Delta T_{S,dec}) & T_S < T_{S,0} + \Delta T_{S,dec} \end{cases}$$

$$\Delta T_H = \begin{cases} 0 & T_H < T_{H,0} + \Delta T_{H,dec} \\ T_H - (T_{H,0} + \Delta T_{H,dec}) & T_H < T_{H,0} + \Delta T_{H,dec}, \end{cases} \quad (10)$$

where $T_{S,0}$ and $T_{H,0}$ represent the initial temperatures in thermoneutral condition [30]. Note that the sweating model in the child is identical to that of the adult, as is demonstrated in section III B.

3) BLOOD PERFUSION RATE

For temperature elevation above a certain level, the blood perfusion rate is increased to carry away the excess heat [13]. The variation in the blood perfusion rate on the skin through vasodilatation is expressed in terms of ΔT_H and ΔT_S as follows:

$$B(\boldsymbol{r}, t) = (B_0(\boldsymbol{r}) + F_{HB}\Delta T_H(t) + F_{SB}\Delta T_S(t)) \cdot 2^{(Tr,t - T_0(r))/6} \quad (11)$$

where B_0 (=3,680 W/m^3/°C) is the basal blood perfusion rate, F_{HB} (=17,500 W/m^3/°C^2) and F_{SB} (=1,100 W/m^3/°C^2) are the weighting coefficients of the signals from the hypothalamus and skin, respectively [17]. Then, ΔT_H and ΔT_S are the changes in the average skin and blood temperature with respect to the respective baseline temperatures.

The variation of the blood perfusion rate in all tissues except for skin at higher temperatures (above 39 °C) is given by the following linear relation[31], [32]:

$$\mathrm{B}(r, t) = \begin{cases} \mathrm{B}_0(r) & T(r, \mathrm{t}) \le 39°\mathrm{C} \\ \mathrm{B}_0(r)[1 + \mathrm{S_B}(\mathrm{T}(r, \mathrm{t}) - 39)] & 39°\mathrm{C} \le T(r, \mathrm{t}) \le 44°\mathrm{C} \\ \mathrm{B}_0(r)\,(1 + 5\mathrm{S_B}) & 44°\mathrm{C} \le T(r, \mathrm{t}) \end{cases} \quad (12)$$

where $B_0(\boldsymbol{r})$ is based on the blood perfusion in each tissue, and S_B(=0.8 °C^{-1}) is a coefficient for determining the changes in the blood perfusion characteristics over time.

D. MODELING SOLAR RADIATION

The finite-difference time-domain (FDTD) method was used for calculating the power absorption in an anatomical human model. An in-house FDTD code, which was validated via inter-comparison, was used [33]. The values of the required dielectric constants of the tissues were empirically obtained [34]. The computational region was truncated by

applying a twelve-layered perfectly matched layer-absorbing boundary.

For harmonically varying fields, the power absorption was calculated from the Joule loss (σE^2 in (1)).

As in [12], solar radiation was simulated considering a realistic scenario. For example, the human models were exposed to two plane waves at $+45$ and -45 degrees from the ground. The former corresponds to sunlight directly irradiating the body and the latter to sunlight reflected from the ground. The incident angle was adjusted to real data. For that angle, a typical power density of the directly incident wave is 1000 W/m^2 [35]. The power density of the reflected wave was estimated as 200 W/m^2 based on a ground reflectance of 0.2 [35]. The power absorption in the models was computed using a resolution of 0.5 mm voxels at 10 GHz, at which wave penetration depth (-2 mm) is approximately the same as the average penetration depth of the electromagnetic wave into the human body in the dominant spectrum (280$-$4000 nm) constituting solar radiation [36]. The power absorption distribution per unit mass is shown in Figure 2. In the present case, the whole-body-averaged energy absorption rate was 5.0 W/kg and 8.5 W/kg for adult and child phantoms, respectively, which are comparable to those estimated from the body surface area multiplied by an incident power density [37].

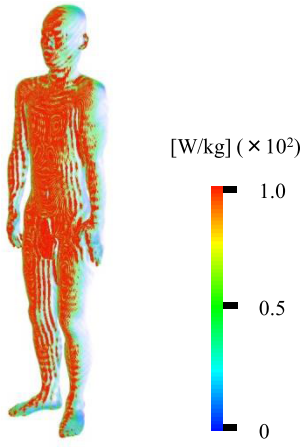

FIGURE 2. Power absorption per unit mass distribution on the adult male model for frontal solar radiation.

E. COMPUTATIONAL IMPLEMENTATION

The computational thermal model was implemented in in-house code written in FORTRAN 95. The bioheat equation (1) and the boundary condition (2) were discretized using a difference method with a six-point stencil in the spatial domain and the explicit Euler method in the time domain. That is, at each time step, the sweating and blood perfusion rates and blood temperature were updated using the temperature distribution calculated at the previous time step. The discretization size was 2 mm in the spatial domain, corresponding to 8 million degrees of freedom, and 2 s in the time domain. It should be noted that the discretization time was chosen so as to satisfy the stability condition in [38].

The SX-ACE supercomputer used for the analysis is a vector-type computer with high vector processing performance of 256 GFLOPS per CPU and high memory bandwidth of 256 GB/s [14]. The latter is essential for large-scale physical computation. To realize speed up on SX-ACE, the code was optimized primarily for vectorization promotion. As will be discussed later, the computation of perspiration, which is one of the factors of thermoregulation, is performed only for the skin tissue, resulting in a conditional branch (if-statement) for discriminating from other tissues. In vector-type computers, such as SX-ACE, successive calculations accompanying this conditional branch may decrease the vectorization rate. The amount of computation for each process depends on the presence or absence of skin tissue (see (7)). This caused imbalance in the computational load between the nodes. Thus, the presence of skin tissue was not decided by conditional branching but by a Boolean function in the position vector $\boldsymbol{r}$. It is noteworthy that this does not perform well on non-vector conventional computers, as the computational cost increases.

F. EXPOSURE SCENARIOS

To verify the code for exercise, children, and the elderly, three different scenarios, whose experimental results have been published, were considered. Comparisons with experimental results were made to verify the difference in the threshold temperature (as observed in the computations) for eliciting a thermoregulatory response, owing to age and body size.

i) The first exposure scenario regarded exercise in younger adults [39]: 1) The subject rested for 90 min in a thermoneutral room with an ambient temperature of 25 °C and relative humidity of 50%; 2) the subject moved and stayed for 90 min in another room whose ambient temperature and relative humidity were 33 °C and 50%, respectively. There, the subject initially sat on a seat for 30 min. Then, the subject walked at 4.5 km/h for 30 minutes using a treadmill, and rested on the seat again for 30 min.

ii) The second scenario regarded younger adults and the elderly [25]: 1) The subject rested in a thermoneutral room with ambient and wall temperature of 28 °C; 2) the ambient temperature was changed gradually from 28 to 40 °C during the first 4 min, and then kept at 40 °C for 86 min.

iii) The final scenario regarded females and children [40]: 1) The subject rested for 10 min in a thermoneutral room with an ambient temperature of 28 °C and relative humidity of 50%; 2) the subject moved and stayed in the exposure chamber whose ambient temperature and relative humidity were 35 °C and 70%, respectively, for 30 min; 3) the subject moved and rested again for 30 min in a recovery room with an ambient temperature of 28 °C and relative humidity of 50%.

G. MODELING BASED ON WHATHER FORECAST DATA

To conduct realistic risk assessment for preventing seasonal heat stroke, the temperature elevation was calculated at ambient heat and solar radiation using weather forecast data. In addition, the absorption of the solar radiation was adjusted to consider the effect of clothing (short sleeve shirts and shorts) [41]. Thus, the whole-body-averaged power absorption rate for solar radiation of adults and children was adjusted to 3.0 W/kg and 5.3 W/kg, respectively. In this study, 10-min weather (temperature and humidity) data were linearly interpolated for use in the computations.

III. COMPUTATIONAL RESULTS

A. COMPUTER IMPLEMENTATION AND ACCELERATION

Figure 3 shows the acceleration for different numbers of processes using code that was speeded up. The speed up was derived from the computational time of single execution of one core for one SX-ACE node (four cores) and that of parallel execution of MPI parallel processing of four processes per node for one node up to 16 nodes (64 processes in parallel). For different numbers of processes, comparison was made under the same exposure condition (model: adult male, exposure time: 3 h, ambient temperature: 37 °C). As shown in Figure 3, the acceleration rate increases as the number of processes increases. Compared to the theoretical value or the maximum number of processes (64), the acceleration rate was improved 55 times by resolving the imbalance, corresponding to a parallelization ratio of 87%.

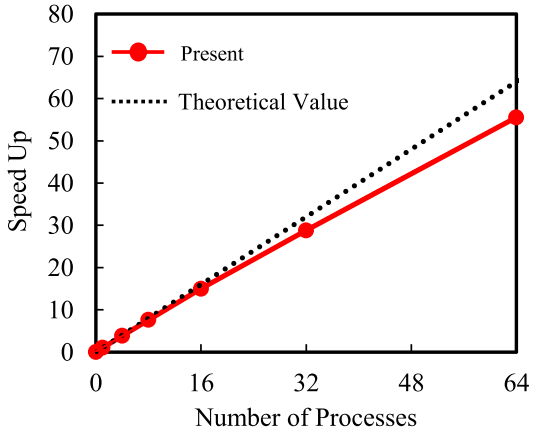

FIGURE 3. Acceleration rate of calculation time vs. number of parallel processes.

In the improved computational algorithm, a large computational load (99.9%) is attributable to physical computation and thermoregulation, namely, 82.2% and 17.7%, respectively. However, before resolving the imbalance of the computation, the corresponding figure was 75.3% (physical computation and thermoregulation were 27.1% and 48.2%, respectively).

B. VALIDATION OF COMPUTATIONAL MODELING

To confirm the effectiveness of the model, the core temperature elevation and sweating computed using the improved bioheat model were compared with measurement data in the literature.

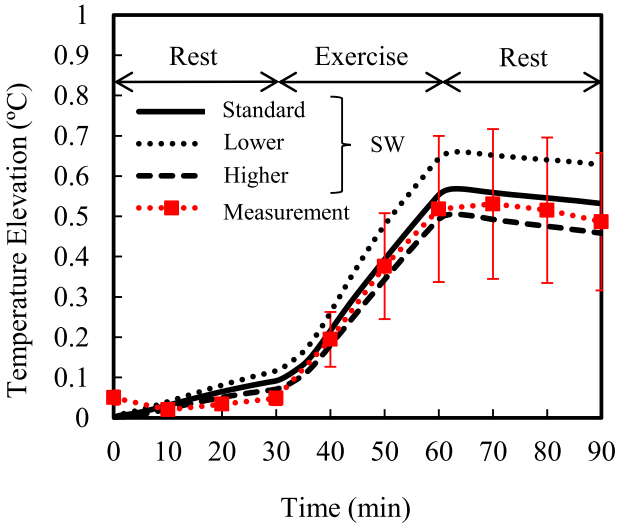

FIGURE 4. Computed and measured core temperature elevations [°C], for exercise tolerance test (33 °C and 50 %). The measured data were obtained from [39]. Error bars represent standard deviation of measured data.

The metabolic equivalent for the treadmill was estimated as 3.5 METs (where 1 MET is the metabolic equivalent of a sedentary person) [39]. As shown in Figure 4, good agreement is observed between the computed and measured core temperature elevation for exercise under heat load. The total water loss in the computation for the normal sweating type was 396.6 g, whereas that in the measurement data was 398.0 g for 90 min. This suggests that the code can effectively simulate thermoregulatory responses of young adults.

Subsequently, the temperature was changed gradually as in [25]. As shown in Figure 5(a), good agreement is observed between the computed and measured core temperature elevation, particularly over time. The core temperature elevation in the computation for the normal sweating type and that in the measurement data for younger adults were 0.49 °C and 0.48 °C, respectively. For elderly, the corresponding figures were 0.70 °C and 0.69 °C. Good agreement is also observed in the time course of the sweating rate, as shown in Figure 5(b). The results suggest that the code can effectively simulate thermoregulatory responses or sweating in the elderly.

In these two validations, three sweating types were used. The results show that the difference in the biological response due to sweating can also be simulated. The third example was concerned with heat exposure based on the experiment in [40]. Figure 6 shows the time course of core temperature elevation in females and eight-month-old children. Good agreement is observed between the computed and measured

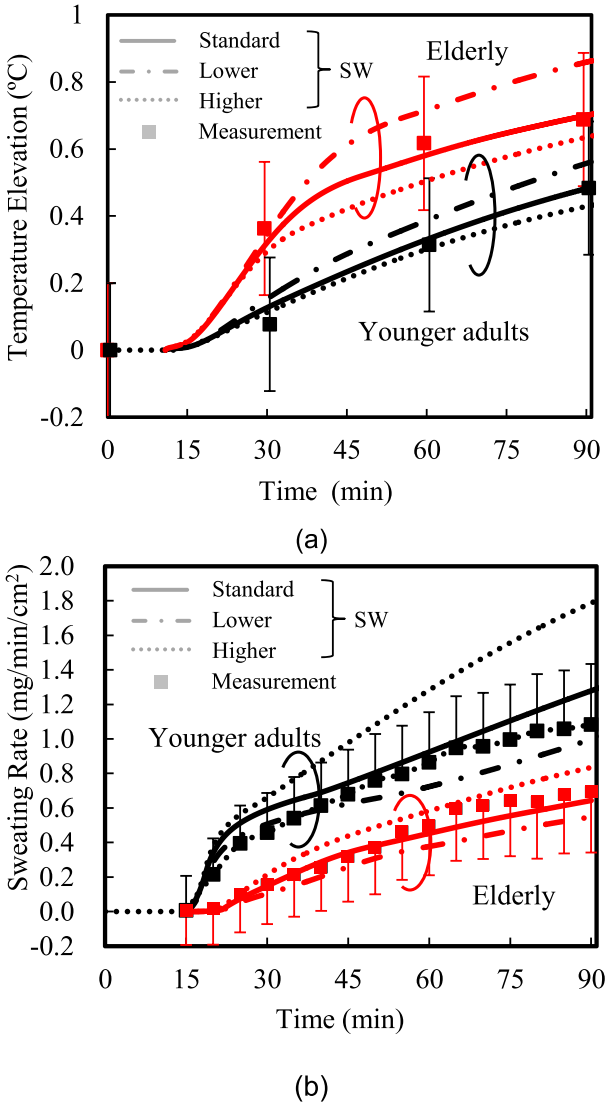

FIGURE 5. Computed and measured (a) core temperature elevations and (b) sweating rates integrated in legs for passive heat exposure (40 °C and 42%). The measured data were obtained from [25]. Error bars represent standard deviation of measured data.

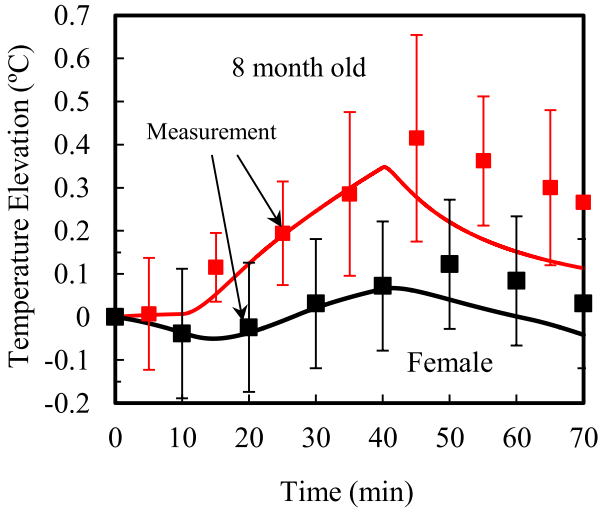

FIGURE 6. Computed and measured core temperature elevations, for heat exposure test (35 °C and 70%). The measured data were obtained from [40]. Error bars represent standard deviation of measured data.

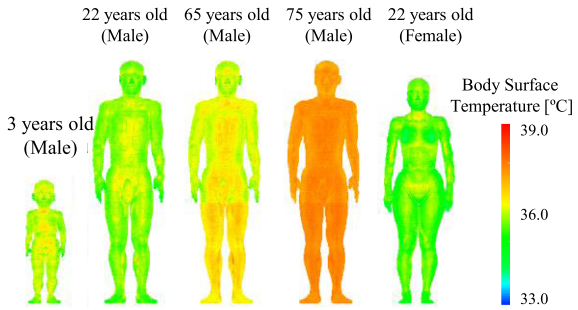

FIGURE 7. Computed temperature distribution on human body surfaces of five models after three hours for given ambient temperature and humidity on July 25, 2015.

core temperature elevation. After the heat exposure (40 min), the computed core temperature decreases in a few minutes, whereas the measured core temperature continues to rise for several minutes.

The reason for this is unclear. However, two possible factors may be the increased metabolism rate when a mother moves from the exposure room to the recovery room while holding her child, and altered heat transfer by contact between the child and the mother. The results suggest that the code is applicable down to eight-month-old children. It is worth noting that the thermoregulation of the child was approximately expressed as identical to that of the young adults.

C. COMPUTATIONAL DEMONSTRATION

Two simulations were conducted to demonstrate risk assessment using this method combined with weather data. In these simulations, the previously measured weather data were used. Figure 7 shows the body surface temperature distribution in different thermoregulatory models for exposure to a certain ambient temperature and humidity without solar radiation, from 10 AM to 1 PM, on July 25, 2015. The body surface temperature of the aged was the highest because the initiation of sweating in the elderly (especially in "aged") is longer compared with young adults, owing to the decline in the thermal sensitivity of the skin due to aging (see (9) and (10)). The difference of the core temperatures in these models was similar to that of the surface temperature; higher in the elderly and children than in young adults.

Likewise, Figure 8 shows the body surface temperature distribution in adults and children for exposure to a certain ambient temperature and humidity with solar radiation, from 1 PM to 2 PM, on July 14, 2016. To simulate walking, the metabolic equivalent of walking was estimated as 3.0 METs [42] in the calculation. The figure shows that the temperature elevation caused by exposure to high ambient temperature, in addition to exercise, was higher in children than in younger adults.

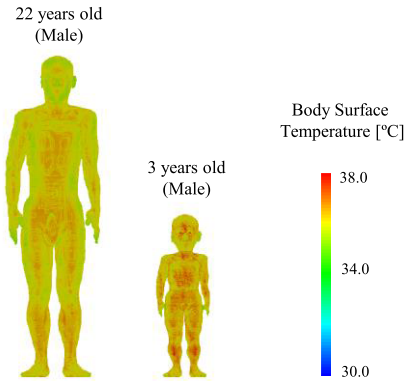

FIGURE 8. Computed temperature distribution on human body surfaces of younger adults and child for 60 min for given ambient temperature and humidity on July 14, 2016.

This is primarily attributed to the difference in the surface area-to-mass ratio between adult and child models. It should be noted that the surface area-to-mass ratio is the dominant factor influencing the core temperature elevation that is due to ambient heat and electromagnetic power absorption [12]. Furthermore, the absorbed energy of the heat transfer from the surrounding air to the body is proportional to the surface area-to-mass ratio. 46 min were required in the child model for a core temperature elevation by 1 °C, which is the suggested limit in [8]. The water loss in 46 min was 390 g, approximately 3% of body weight, which is a measure of dehydration; in 1 h, it was 530 g, approximately 4% of body weight.

D. WEB-BASED APPLICATION

A database for core temperature elevation and sweating was developed for typical Japanese weather data for the duration of one hour. 104 combinations of ambient temperature (from 28 to 40 °C per 1 °C) and relative humidity (from 10 to 80% per 10%) were chosen. For these scenarios, four human body models, young adult, older adult, child, and infant, were considered. 7296 simulations were conducted and used for generating the database.

On the webpage (see Figure 9. translated), users choose their age and activity level, and their location is acquired by the global positioning system (https://www.netsuzero.jp/selfcheck). The corresponding weather data is then estimated. The output consists of the recommended water intake, based on the water loss, and the allowable duration of activity for preventing excess core temperature elevation, as suggested in ACGIH [8]. Considering individual differences, the unit of water loss is 100 (half a glass of water), 200 (two glasses), 500 (a bottle), 1,000 ml (two bottles), and more than 1,000 ml (more than two bottles). The allowable duration of activity is a multiple of 15 min.

This application was deployed in April 2017, had 170,640 page views from April 2017 to September 2017.

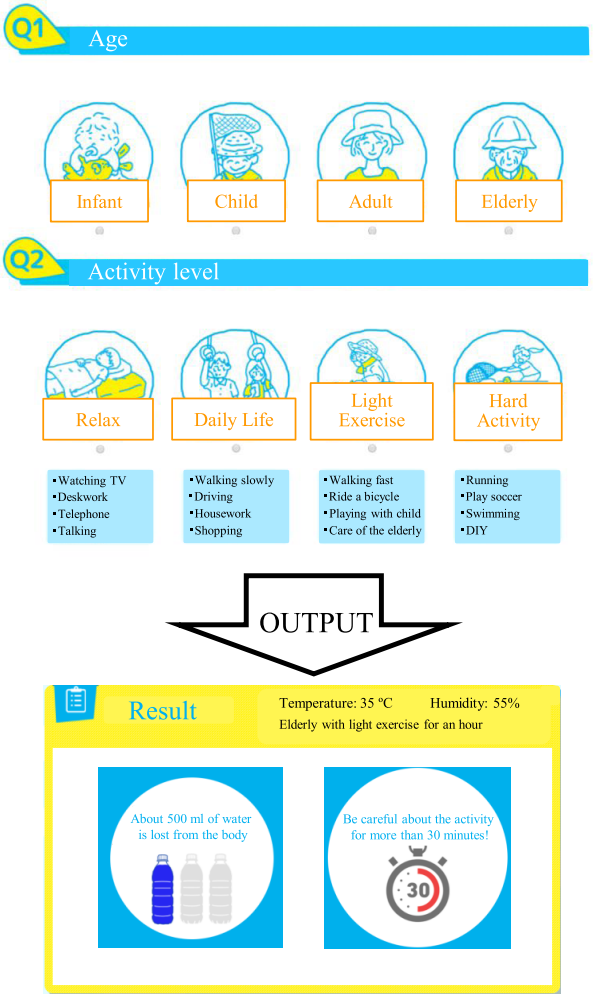

FIGURE 9. Schematic explanation of the web-based system. When users choose age, activity level, and location (for weather data), water loss and allowable duration of the activity are displayed.

IV. DISCUSSION

A. COMPUTATIONAL IMPLEMENTATION

The code was implemented on an SX-ACE supercomputer, a vector-type computer, which has high vector processing performance of 256 GFLOPS per CPU and high memory bandwidth of 256 GB/s [14]. The latter feature is suitable for large-scale physical computation. Moreover, it should be stressed that the code involved not only thermodynamics but also the thermoregulatory response. Thus, efficient implementation on a vector-type computer was challenging. It should also be note that the code for modeling electromagnetics was also used for modeling solar radiation. However, this is not discussed here because there was no obstacle in its implementation.

The original computational time for a three-hour exposure to thermal load was 16 h on a workstation (CPU: Intel®Xeon®W5590 @3.33GHz, 4×2 cores), which was accelerated to 77 s in the adult model and 17 s in the child model on the supercomputer with 64 cores. This allowed

the evaluation of temperature elevation and sweating in less than 10 min, even considering the variation of sweating rate covering approximately 90% of the population (see the discussion below). The difference with the theoretical value in speed up (Figure 3) would be attributable to initial value setting, processing time of non-parallelized parts such as file I/O, and data synchronization delay owing to data communication between nodes.

To confirm the applicability of the code in common experimental scenarios, three exposure cases were considered. The reason for choosing these examples was to simulate exercise as well as the elderly and children. In all cases, the code simulated the scenarios in good agreement with measured data. However, some difference was observed in the early stages of exposure because thermoneutral conditions are different for different subjects, and, initially, the ambient temperature does not always provide thermoneutral conditions. As seen from (7), the core and mean skin temperature elevations affect sweating rate, resulting in similar trends.

B. UNCERTAINTY FACTORS

It is difficult to determine the population coverage in the application of the system. The variability of core temperature elevation and water loss is primarily attributable to sweating rate and body shape, which is characterized by the body surface area-to-mass ratio. This is evident from the empirical formula (9) [12] for estimating core temperature elevation.

Regarding the effect of the body shape, it was clarified that the dominant factor affecting core temperature elevation was approximately proportional to the body surface-area-to-mass ratio for passive heat exposure [12]. The limitation of using one anatomical model is that the surface-area-to-mass ratio is fixed. This analysis was validated by a comparison with measured data obtained from [25]. The mean surface-area-to-mass ratio for 15 younger and older subjects was estimated as 0.0256 and 0.0242 m^2/kg, respectively [43]. Moreover the surface area in Table 1 was estimated based on Du Bois and Du Bois [43]. The mean surface-area-to-mass ratio for the younger and older subjects is smaller than that of the numerical Japanese male model by 6.5% and 11%, respectively. To cover 90% of the population, core temperature elevation can be estimated by these factors; up to 20% to cover two standard deviations.

The second factor was considered as much as possible to ensure that the parameters listed in Table 3 cover all the data for younger adults. Moreover, the degradation of the temperature sensor in the hypothalamus, which is obvious at the age of approximately 75 years or over, was not considered [23]. If need be, these effects can be easily considered by changing the parameters in (9) (see Figures 4 and 5). The sweating response is not as available as body shape. However, low and high sweating rates were estimated to cover nearly all the measured data presented in [13] (some of them are within standard deviation); thus they are expected to cover at least 68% (standard deviation) but less than 95% (two standard deviations).

Additional uncertainty exists for children, as no measured data has been reported for core temperature elevation higher than 0.5−0.6 °C. One of the additional factors not considered here is the decline of sweating rate caused by disease (e.g., diabetes). This decline is primarily attributed to the degradation of the thermal sensitivity of the skin. Further, the thermoregulatory model is based on individuals living in the temperature zone. The arctic and tropical zones were not considered.

C. APPLICATION

As a pilot study, the water loss and core temperature elevation were estimated for two scenarios using the same weather data. The computation suggested the effectiveness of the classification into adults, children, and the elderly. As the data for the adult male and female models were quite similar, or within individual variability, the data of the male model was chosen for estimating heat stroke risk. A more detailed version of this computation can be used in large events using weather forecast data. The database was developed for a large number of studies and has been used extensively.

V. CONCLUSIONS

A fast computation for simulating temperature elevation and sweating was implemented for risk management of heat stroke. The computational time for covering more than 90% of the population in Japan is less than 10 min. The system may be used in large events in summer and for more case-specific risk assessment. As a pilot study, a web-based risk assessment application was developed and has been used since 2017. It had 170,640 page views from April 2017 to September 2017. In the future, it could be improved so that it may have worldwide population coverage (e.g.,the subarctic and torrid zone) based on thermophysiological data.

REFERENCES

[1] G. A. Meehl and C. Tebaldi, "More intense, more frequent, and longer lasting heat waves in the 21st century," *Science*, vol. 305, no. 5686, pp. 994–997, Aug. 2004.
[2] Deptartment of Environmental Health, Ministry of Environment, "Heat stroke, manual of environmental health," (in Japanese), Dept. Environ. Health, MOE, Singapore, Tech. Rep., 2014. [Online]. Available: http://www.wbgt.env.go.jp/pdf/envman/full.pdf
[3] Fire and Disaster Management Agency, Ministry of Internal Affairs and Communications, "Emergency transportation status due to heat stroke in Heisei 28," (in Japanese), *Materials*, 2016. [Online]. Available: http://www.fdma.go.jp/neuter/topics/houdou/h28/10/281012_houdou_2.pdf
[4] S. Guergova and A. Dufour, "Thermal sensitivity in the elderly: A review," *Ageing Res. Rev.*, vol. 10, no. 1, pp. 80–92, 2011.
[5] S. F. Wetterhall, D. M. Coulombier, J. M. Herndon, S. Zaza, and J. D. Cantwell, "Medical care delivery at the 1996 Olympic Games," *Jama*, vol. 279, no. 18, pp. 1463–1468, 1998.
[6] G. M. Budd, "Wet-bulb globe temperature (WBGT)—Its history and its limitations," *J. Sci. Med. Sport*, vol. 11, no. 1, pp. 20–32, 2008.
[7] P. Bröde *et al.*, "Deriving the operational procedure for the universal thermal climate index (UTCI)," *Int. J. Biometeorol.*, vol. 56, no. 3, pp. 481–494, 2012.
[8] *Heat Stress and Strain*, ACGIH, Cincinnati, OH, USA, 2017.
[9] D. Fiala, K. J. Lomas, and M. Stohrer, "Computer prediction of human thermoregulatory and temperature responses to a wide range of environmental conditions," *Int. J. Biometeorol.*, vol. 45, no. 3, pp. 143–159, 2001.
[10] K. R. Foster and E. R. Adair, "Modeling thermal responses in human subjects following extended exposure to radiofrequency energy," *Biomed. Eng. OnLine*, vol. 3, no. 1, p. 4, 2004.

[11] A. Hirata, T. Nomura, and I. Laakso, "Computational estimation of body temperature and sweating in the aged during passive heat exposure," *Int. J. Thermal Sci.*, vol. 89, pp. 154–163, Mar. 2015.
[12] R. Hanatani, I. Laakso, A. Hirata, M. Kojima, and H. Sasaki, "Dominant factors affecting temperature elevation in adult and child models exposed to solar radiation in hot environment," *Prog. Electromagn. Res. B*, vol. 34, pp. 47–61, Jan. 2011.
[13] J. A. J. Stolwijk, "A mathematical model of physiological temperature regulation in man," NASA, Washington, DC, USA, Tech. Rep. NASA-CR-1855, 1971.
[14] R. Egawa *et al.*, "Potential of a modern vector supercomputer for practical applications: Performance evaluation of SX-ACE," *J. Supercomput.*, vol. 73, no. 9, pp. 3948–3976, 2017.
[15] T. Nagaoka, S. Watanabe, K. Sakurai, E. Kunieda, M. Taki, and Y. Yamanaka, "Development of realistic high-resolution whole-body voxel models of Japanese adult males and females of average height and weight, and application of models to radio-frequency electromagnetic-field dosimetry," *Phys. Med. Biol.*, vol. 49, no. 1, pp. 1–15, 2004.
[16] H. H. Pennes, "Analysis of tissue and arterial blood temperatures in the resting human forearm," *J. Appl. Physiol.*, vol. 1, no. 2, pp. 93–122, 1948.
[17] P. Bernardi, M. Cavagnaro, S. Pisa, and E. Piuzzi, "Specific absorption rate and temperature elevation in a subject exposed in the far-field of radio-frequency sources operating in the 10–900-MHz range," *IEEE Trans. Biomed. Eng.*, vol. 50, no. 3, pp. 295–304, Mar. 2003.
[18] A. Hirata and O. Fujiwara, "Modeling time variation of blood temperature in a bioheat equation and its application to temperature analysis due to RF exposure," *Phys. Med. Biol.*, vol. 54, no. 10, pp. N189–N196, 2009.
[19] A. Hirata, T. Asano, and O. Fujiwara, "FDTD analysis of body-core temperature elevation in children and adults for whole-body exposure," *Phys. Med. Biol.*, vol. 53, no. 18, pp. 5223–5238, 2008.
[20] M. Rida, N. Ghaddar, K. Ghali, and J. Hoballah, "Elderly bioheat modeling: Changes in physiology, thermoregulation, and blood flow circulation," *Int. J. Biometeorol.*, vol. 58, no. 9, pp. 1825–1843, 2014.
[21] D. Fiala, K. J. Lomas, and M. Stohrer, "A computer model of human thermoregulation for a wide range of environmental conditions: The passive system," *J. Appl. Physiol.*, vol. 87, no. 5, pp. 1957–1972, 1999.
[22] T. Samaras, A. Christ, and N. Kuster, "Effects of geometry discretization aspects on the numerical solution of the bioheat transfer equation with the FDTD technique," *Phys. Med. Biol.*, vol. 51, no. 11, p. N221-9, 2006.
[23] G. S. Anderson, G. S. Meneilly, and I. B. Mekjavic, "Passive temperature lability in the elderly," *Eur. J. Appl. Physiol. Occupat. Physiol.*, vol. 73, nos. 3–4, pp. 278–286, 1996.
[24] Y. Nishi and A. P. Gagge, "Direct evaluation of convective heat transfer coefficient by naphthalene sublimation," *J. Appl. Physiol.*, vol. 29, no. 6, pp. 830–838, 1970.
[25] A. Dufour and V. Candas, "Ageing and thermal responses during passive heat exposure: Sweating and sensory aspects," *Eur. J. Appl. Physiol.*, vol. 100, no. 1, pp. 19–26, 2007.
[26] Y. Inoue and M. Shibasaki, "Regional differences in age-related decrements of the cutaneous vascular and sweating responses to passive heating," *Eur. J. Appl. Physiol. Occupat. Physiol.*, vol. 74, nos. 1–2, pp. 78–84, 1996.
[27] Y. Inoue, M. Shibasaki, H. Ueda, and H. Ishizashi, "Mechanisms underlying the age-related decrement in the human sweating response," *Eur. J. Appl. Physiol. Occupat. Physiol.*, vol. 79, no. 2, pp. 121–126, 1999.
[28] Y. Tochihara, T. Kumamoto, J.-Y. Lee, and N. Hashiguchi, "Age-related differences in cutaneous warm sensation thresholds of human males in thermoneutral and cool environments," *J. Thermal Biol.*, vol. 36, no. 2, pp. 105–111, 2011.
[29] A. Hirata, T. Nomura, and I. Laakso, "Computational estimation of decline in sweating in the elderly from measured body temperatures and sweating for passive heat exposure," *Physiol. Meas.*, vol. 33, no. 8, pp. N51–N60, 2012.
[30] E. R. Adair and D. R. Black, "Thermoregulatory responses to RF energy absorption," *Bioelectro Magn.*, vol. 24, no. S6, pp. S17–S38, 2003.
[31] M. Hoque and O. P. Gandhi, "Temperature distributions in the human leg for VLF-VHF exposures at the ANSI-recommended safety levels," *IEEE Trans. Biomed. Eng.*, vol. BME-35, no. 6, pp. 442–449, Jun. 1988.
[32] I. Chatterjee and O. P. Gandhi, "An inhomogeneous thermal block model of man for the electromagnetic environment," *IEEE Trans. Biomed. Eng.*, vol. BME-30, no. 11, pp. 707–715, Nov. 1983.
[33] P. J. Dimbylow, A. Hirata, and T. Nagaoka, "Intercomparison of whole-body averaged SAR in European and Japanese voxel phantoms," *Phys. Med. Biol.*, vol. 53, no. 20, pp. 5883–5897, 2008.
[34] S. Gabriel, R. W. Lau, and C. Gabriel, "The dielectric properties of biological tissues: III. Parametric models for the dielectric spectrum of tissues," *Phys. Med. Biol.*, vol. 41, no. 11, pp. 2271–2293, 1996.
[35] *Standard Tables for Reference Solar Spectral Irradiances: Direct Normal and Hemispherical on 37Âř Tilted Surface*, Standard ASTM G173-03, 2012.
[36] International Commission on Non-Ionizing Radiation Protection, "ICNIRP statement on far infrared radiation exposure," *Health Phys.*, vol. 91, no. 6, pp. 630–645, 2006.
[37] K. Kubaha, D. Fiala, J. Toftum, and A. H. Taki, "Human projected area factors for detailed direct and diffuse solar radiation analysis," *Int. J. Biometeorology*, vol. 49, no. 2, pp. 113–129, 2004.
[38] J. Wang and O. Fujiwara, "FDTD computation of temperature rise in the human head for portable telephones," *IEEE Trans. Microw. Theory Techn.*, vol. 47, no. 8, pp. 1528–1534, Aug. 1999.
[39] H. Enomoto *et al.*, "Effects of water intake on human responses in a hot working environment," *J. Occupat. Safety Health*, vol. 4, no. 1, pp. 7–13, 2011.
[40] K. Tsuzuki-Hayakawa, Y. Tochihara, and T. Ohnaka, "Thermoregulation during heat exposure of young children compared to their mothers," *Eur. J. Appl. Physiol. Occupat. Physiol.*, vol. 72, nos. 1–2, pp. 12–17, 1995.
[41] H. F. Blum, "The solar heat load: Its relationship to total heat load and its relative importance in the design of clothing," *J. Clin. Invest.*, vol. 24, no. 5, pp. 712–721, 1945.
[42] M. Jette, K. Sidney, and G. Blümchen, "Metabolic equivalents (METS) in exercise testing, exercise prescription, and evaluation of functional capacity," *Clin. Cardiol.*, vol. 13, pp. 555–565, Aug. 1990.
[43] D. D. Bois and E. F. D. Bois, "Clinical calorimetry: Tenth paper a formula to estimate the approximate surface area if height and weight be known," *Arch. Internal Med.*, vol. 17, p. 863, Jun. 1916.

KAZUYA KOJIMA received the B.E. degree in electrical and electronic engineering from the Nagoya Institute of Technology, Nagoya, Japan, in 2016, where he is currently pursuing the master's degree.

His current research interests include thermodynamics and thermoregulation modeling in human related to heat-related illness.

AKIMASA HIRATA (S'98–M'01–SM'10–F'17) received the B.E., M.E., and Ph.D. degrees in communications engineering from Osaka University, Suita, Japan, in 1996, 1998, and 2000, respectively.

He was a Visiting Research Scientist with the University of Victoria, Victoria, BC, Canada, in 2000. In 2001, he joined the Department of Communications Engineering, Osaka University, as an Assistant Professor. In 2004, he joined the Department of Computer Science and Engineering, Nagoya Institute of Technology, as an Associate Professor, where he is currently a Full Professor. His research interests include electromagnetics and thermodynamics in biological tissue, waveguide analysis, EMC and EMI, and computational techniques in electromagnetics.

Prof. Hirata is a fellow of the Institute of Physics, and a member of IEICE, IEE Japan, and the Bioelectromagnetics Society. He is an Expert of World Health Organization. He is an editorial board member of physics in medicine and biology. He received several awards, including the Young Scientists' Prize (2006) and the Prizes for Science and Technology (Research Category 2011, Public Understanding Promotion Category 2014) by the Commendation for Science and Technology, Minister of Education, Culture, Sports, Science and Technology, Japan, the IEEE EMC-S Technical Achievement Award (2015), and the Japan Academy Medal (2018). He is a Chair of project group of International Commission on Non-Ionizing Radiation Protection and a Subcommittee (EMF Dosimetry Modeling) Chair of the IEEE International Committee on Electromagnetic Safety. From 2006 to 2012, he was also an Associate Editor of the IEEE TRANSACTIONS ON BIOMEDICAL ENGINEERING.

KAZUMA HASEGAWA received the B.E. degree in electrical and electronic engineering from the Nagoya Institute of Technology, Nagoya, Japan, in 2016, where he is currently pursuing the master's degree.

His current research interests include human protection from radio-frequency and optical radiation and environmental heat.

SACHIKO KODERA received the B.E. and M.E. degrees in electrical and computer engineering from the Nagoya Institute of Technology, Nagoya, Japan, in 2002 and 2006, respectively.

In 2016, she joined the Department of Electrical and Mechanical Engineering, Nagoya Institute of Technology, as a Researcher. Her current research interests include electromagnetic and thermal dosimetry modeling in humans for radio-frequency and ambient heat exposures.

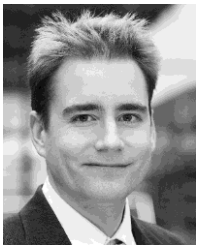

ILKKA LAAKSO (M'14) received the M.Sc. (Tech.) degree in electromagnetics from the Helsinki University of Technology, Espoo, Finland, in 2007, and the D.Sc. (Tech.) degree in electromagnetics from Aalto University, Espoo, Finland, in 2011.

From 2013 to 2015, he was a Research Assistant Professor and a Research Associate Professor with the Department of Computer Science and Engineering, Nagoya Institute of Technology. Since 2015, he has been an Assistant Professor in electromagnetics with Health Technology, Aalto University. He has authored over 80 papers published in international journals and conference proceedings. His current research interests include computational bioelectromagnetic modeling for assessment of human safety and biomedical applications.

Prof. Laakso is a member of the Scientific Expert Group with the International Commission on Non-Ionizing Radiation Protection. He received several awards, including the Student Award in International Symposium on EMC, Kyoto, in 2009, the Ericsson Young Scientist Award in 2011, and the Young Scientist Award in URSI General Assembly and Scientific Symposium, Montreal, Canada, in 2017. He is the Secretary and a Working Group Chair of Subcommittee of EMF Dosimetry Modeling of the IEEE International Committee on Electromagnetic Safety.

DAISUKE SASAKI received the B.E. degree in engineering from Yamagata University in 2006. He is currently a Technical Staff of information bureau with Tohoku University. He is involved in user support/system operation service at the Cyberscience Center.

TAKESHI YAMASHITA received the B.E. and master's degrees in material engineering from Tohoku University in 2000 and 2002, respectively. He is currently a Technical Specialist of information bureau with Tohoku University. He is involved in user support/system operation at the Cyberscience Center.

RYUSUKE EGAWA received the B.E. and master's degrees in information sciences from Hirosaki University in 1999 and 2001, respectively, and the Ph.D. degree in information sciences from Tohoku University in 2004.

He is currently an Associate Professor with the Cyber science Center, Tohoku University. His research interests include high-performance/low-power computer architectures and their HPC applications.

Prof. Egawa is a member of the IEEE CS, IEICE, and IPSJ.

YUKA HORIE received the B.Sc. and M.Sc. degrees in geography from Tokyo Metropolitan University, Hachioji, Japan, in 2004 and 2006, respectively.

Since 2009, she has been with the Japan Weather Association. One of her main work is to propose new project and design systems about heatstroke. These are advanced weather information which relates human daily life to weather. She is also an Expert of biometeorology.

NANAKO YAZAKI received the bachelor's degree in business administration from Meiji University, Tokyo, Japan, in 2007.

She has been a Project Leader of the Education Project of Heatstroke Prevention (Heatstroke Zero) since 2016. Since 2015, she has been with the Japan Weather Association. To promote heatstroke project and weather information effectively, she develops various techniques and makes new business plan with the skill of marketing communication.

SAERI KOWATA received the B.Sc. degree in geosystem sciences from Nihon University, Tokyo, Japan, in 2009.

Since 2016, she has been with the Japan Weather Association. She participates in the Education Project of Heatstroke Prevention (Heatstroke Zero). She takes charge of system design of official web site and UI/UX.

KENJI TAGUCHI received the B.E., M.E., and Ph.D. degrees in electrical and electronic engineering from the Kitami Institute of Technology, Kitami, Japan, in 2001, 2003, and 2006, respectively.

From 2006 to 2009, he joined the Department of Information and Communication Engineering, Kumamoto National College of Technology, as a Research Associate. Since 2009, he has been an Associate Professor with the Department of Electrical and Electronic Engineering, Kitami Institute of Technology. His research interests include the analysis of electromagnetic fields, electromagnetic compatibility, and optimization of microwave circuits.

TATSUYA KASHIWA (M'88) was born in Hokkaido, Japan, in 1961. He received the B.S. and M.S. degrees in electrical engineering from Hokkaido University, Hokkaido, Japan, in 1984 and 1986, respectively, and the D.Eng. degree from Hokkaido University.

He was an Assistant Professor with the Department of Electrical Engineering in 1988. He was an Associate Professor with the Department of Electrical and Electronic Engineering, Kitami Institute of Technology, in 1996, where he has been a Professor since 2008. He has co-authored the books *Handbook of Microwave Technology* (Academic Press) and *Antennas and Associated Systems for Mobile Satellite Communications* (Research Signpost). His research interests include the analysis of electromagnetic fields, electromagnetic compatibility, acoustic fields, and optimization of microwave circuits.

Prof. Kashiwa was a member of technical committee on electromagnetic theory and microwaves of IEICE. He is a member of IEEJ and a fellow of IEICE. He received the IEEE AP-S Tokyo Chapter Young Engineer Award in 1992. He was the Chairman of technical committee on electronics simulation technology (EST).